Inactivation of PTEN and ZFHX3 in Mammary Epithelial Cells Alters Patterns of Collective Cell Migration

Ali Dayoub, Artem Fokin, Maria Lomakina, John James, Marina Plays, Tom Jacquin, Nikita Novikov, Rostislav Vorobyov, Anastasia Schegoleva, Karina Rysenkova, et al.

Article

Inactivation of PTEN and ZFHX3 in mammary epithelial cells alters patterns of collective cell migration

Ali Dayoub [1,2,3], Artem I. Fokin [2], Maria E. Lomakina [1], John James [2], Marina Plays [2], Tom Jacquin [2], Nikita M. Novikov [2,4], Rostislav S. Vorobyov [4], Anastasia A. Schegoleva [4], Sergey V. Leonov [3], Evgeny V. Denisov [4], Alexis M. Gautreau [2, *] and Antonina Y. Alexandrova [1, *]

[1] N.N. Blokhin Cancer Research Center of the Ministry of Health of the Russian Federation, 115478 Moscow, Russia
[2] Ecole Polytechnique, Institut Polytechnique de Paris, Palaiseau, France
[3] Moscow Institute of Physics and Technology, Moscow, Russia
[4] Cancer Research Institute, Tomsk National Research Medical Center, Russian Academy of Sciences, Tomsk, 634009 Tomsk, Russia
* Correspondence: alexis.gautreau@polytechnique.edu (A.M.G.); tonya_alex@yahoo.com (A.Y.A.)

Abstract: Whole exome sequencing of invasive mammary carcinomas revealed association of mutations in *PTEN* and *ZFHX3* tumor suppressor genes (TSGs). We generated single and combined *PTEN* and *ZFHX3* knock-outs (KOs) in the immortalized mammary epithelial cell line MCF10A to study the role of these genes and their potential synergy in migration regulation. Inactivation of *PTEN*, but not *ZFHX3*, induced the formation of large colonies in soft agar. *ZFHX3* inactivation in *PTEN* KO, however, increased colony numbers and normalized their size. Cell migration was affected in different ways upon *PTEN* and *ZFHX3* KO. Inactivation of *PTEN* enhanced coordinated cell motility and thus collective migration of epithelial islets and wound healing. In contrast, *ZFHX3* knockout resulted in the acquisition of uncoordinated cell movement associated with the appearance of immature adhesive junctions (AJs) and increased expression of the mesenchymal marker vimentin. Inactivation of the two TSGs thus induce different stages of partial epithelial-to-mesenchymal transitions (EMT). Upon double KO (DKO), cells displayed still another motile state, characterized by a decreased coordination in collective migration and high levels of vimentin, but a restoration of mature linear AJs. This study illustrates the plasticity of migration modes of mammary cells transformed by a combination of cancer-associated genes.

Keywords: Cell migration, Epithelial-to-Mesenchymal Transition, partial EMT, vimentin, E-cadherin, adherens junctions.

1. Introduction

The understanding of molecular mechanisms responsible for tumor progression have greatly benefited from Next Generation Sequencing (NGS) of tumors. Nowadays, Whole Exome Sequencing (WES) represents a fast and reliable way to identify the majority of mutations affecting cancer-associated genes. It also paves the way to precision medicine of cancers, which reveals prognosis and suggest treatments of cancers based on the mutations that the tumor harbors. The most deadly phase of cancer is when tumor cells disseminate throughout the organism and seed distant metastases. Despite initial expectations to identify genes specifically promoting migration and invasion of tumor cells, it appeared that most cancer-associated genes promoting cell migration also promote proliferation in a pleiotropic and perhaps even coupled manner [1,2].

Our understanding of tumor cell dissemination has greatly improved and simultaneously complexified. EMT, where non-mobile polarized epithelial cells with

developed cell-cell adhesions turn into highly mobile individual mesenchymal cells, has been observed in the progression of a number of carcinomas [3]. It is now clear, however, that this process is not limited to the manifestation of the two extreme states of cells, epithelial versus mesenchymal, but is rather multistep with a series of changes during which cells gradually lose their epithelial characteristics and acquire properties of mesenchymal cells. The main feature of full EMT is the complete downregulation of E-cadherin mediated AJs. The early stages of EMT are not associated with a significant downregulation of E-cadherin but accompanied by significant rearrangement of AJs [4-7]. Developed E-cadherin AJs are compact and appear as a single E-cadherin line, referred to as linear or tangential AJs, whereas disparate non-linear AJs can be represented by individual E-cadherin dots combined into a dotted line (punctuated AJs) or by radial stripes (radial AJs). Reorganization of the AJ indicates a weakening of cell-cell interactions and the acquisition of a mobile phenotype by cells. Cells retain cell–cell adhesions, the main characteristic of epithelial cells, while acquiring migratory abilities, in a process called partial, or hybrid EMT [8,9]. Such partial EMTs lead to collective migration [10-12] and proved to be more capable of forming tumors than complete EMTs [13]. Carcinoma cells in the partial EMT state more efficiently metastasize than cells with a fully epithelial or mesenchymal phenotype [4,5,8,14]. Numerous cancer driver genes have been reported to enhance migration and invasion of tumor cells [15], yet how these genes cooperate to produce a given mode of migration has been poorly studied.

PTEN (Phosphatase and tensin homolog) is frequently deleted in many cancers, such as glioblastoma, breast, lung, colon and prostate cancer [16-18]. Hemizygous *PTEN* deletions were associated with poor prognosis of mammary carcinomas [16]. In addition to the classical loss of heterozygosity (LOH) in tumors, *PTEN* gene is also frequently silenced by epigenetic factors during tumor progression [16,19-21]. *PTEN* loss induced EMT in tumor cells of colon cancer [22], prostate cancer [23] and breast cancer [24,25]. PTEN inactivation was also reported to increase collective migration of non-tumor cells both in vitro and in vivo [26]. Downregulation of *PTEN* enhanced cell migration and wound healing of human corneal epithelial cell monolayers and rat cornea scratch wound models as well as in the model of wound healing of whole rat eyes [27].

ZFHX3 (Zinc finger homeobox protein 3), also known as ATBF1 (AT motif binding factor 1), is a transcription factor that was implicated in myogenic differentiation, cell proliferation and embryogenesis [28,29]. It is a TSG in multiple types of cancers, and its genomic deletion or mRNA downregulation promotes the prostate, breast, head and neck, and gastric cancer progression [30]. In epidermal keratinocytes, *ZFHX3* downregulation promotes cell migration and EMT traits, such as the loss of E-cadherin mediated junctions and their replacement by N-cadherin mediated junctions [31]. The transcription factor *ZFHX3* is rarely mutated, but its mRNA expression level is almost systematically reduced in breast cancer cell lines [32,33]. Moreover, low levels of ZFHX3 are strongly correlated with poor prognosis of breast cancer patients [33].

Here we studied the combination of these two TSGs (*PTEN* and *ZFHX3*) that are indeed found mutated simultaneously in the same invasive mammary carcinomas. To understand their contribution to cell transformation and migration, we inactivated these two genes in an immortalized, but untransformed mammary epithelial cell line, MCF10A.

2. Results

2.1. Single and combined KOs of genes found altered in mammary carcinomas

We performed a small sequencing project of 10 invasive mammary carcinomas by whole exome sequencing. In the list of mutations found in the tumor, but not in the soma of patients, we identified putative driver mutations by comparing with the list of cancer driver genes curated by oncoKB (oncoKB.org). We found several occurrences of well-established driver genes of breast cancer, such as *PIK3CA* and *PTEN*. We noticed

that *PTEN* alteration was combined with *ZFHX3* alteration in 2 out of the 10 tumors. We wondered if the combination of these two driver mutations was indicative of a synergy between the two driver genes. Indeed *PTEN* and *ZFHX3* are mutated in 5.9 % and 3.0 % of tumors, respectively (cBioportal on TCGA cohort) rendering their association at random unlikely. Therefore we decided to study their potential synergy by deriving single and combined KOs in the MCF10A cell line, originating from a human fibrotic breast and that is immortalized, but not transformed [34]. *PTEN* KO in MCF10A was commercially available. We generated biallelic KO of *ZFHX3* in parental MCF10A and in the *PTEN* KO (Figure S1). Thus, we study here a series of 4 cell lines, parental MCF10A, single KO of *PTEN* and *ZFHX3* and the double KO of both genes (DKO).

2.2. Morphology alterations caused by PTEN and ZFHX3 KOs

MCF10A cells in tissue culture dishes display variable morphologies. Epithelial islets usually co-exist with isolated cells. *PTEN* KO led to a pronounced epithelial phenotype with rare isolated cells. On the contrary, in *ZFHX3* KO cultures, the epithelial morphology is less defined and more isolated cells are present. This effect of *ZFHX3* inactivation is reversed when combined with *PTEN* KO (Figure 1).

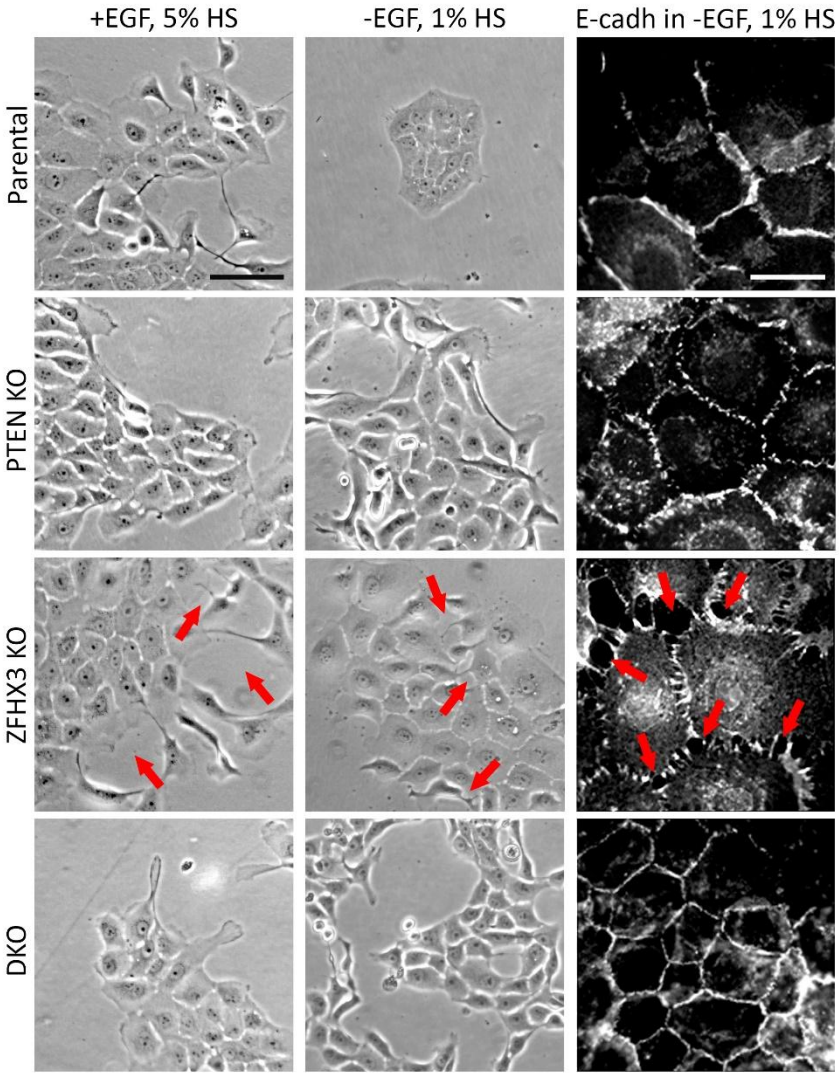

Figure 1. Morphology of genome-edited MCF10A cells in full or depleted medium. Phase contrast view and E-cadherin immunofluorescence. HS: Horse serum. Red arrows point to gaps between cell–cell contacts, Scale bars 100 μm for phase contrast pictures and 20 μm for immunofluorescence.

The incubation of cells in depleted medium (without EGF and with only 1% horse serum) potentiated the epithelial phenotype in control cells and such conditions will be used below to analyze the contribution of each mutation to the migration pattern of mammary epithelial cells. In these conditions, parental MCF10A cells form islets in sparse culture and isolated cells are practically absent. In depleted medium, the morphology of *PTEN* KO cells did not change significantly from the one observed in full medium; *ZFHX3* KO formed loose islets consisting of well spread cells and gaps between cells (red arrows in Figure 1), also some individual cells scattered from groups. DKO cells were aggregated in small islets (Figure 1). To evaluate cell-cell contacts in these cultures, we stained cells for E-cadherin. Control MCF10A cells in condition of depleted medium formed typical linear E-cadherin Adherens Junctions (AJs), tangential to cell boundaries of the tight islets (Figure 1). In sharp contrast, *ZFHX3* KO islets displayed radial AJs. *PTEN* KO cells displayed punctuate AJs looking like dashed lines. The two single KO thus exhibited rearranged AJs. Yet the DKO line exhibited linear AJs looking like the ones of parental cells.

Since *PTEN* and *ZFHX3* are two described cancer driver genes, we wanted to evaluate the level of transformation that these genetic alterations provide to untransformed MCF10A cells. To this end, we tested the ability of the genome edited cells to grow colonies in soft agar. After 3 weeks of anchorage independent growth, parental MCF10A cells formed only rare and small colonies. In contrast, *PTEN* KO cells formed colonies of various sizes, some of them being very large (Figure 2).

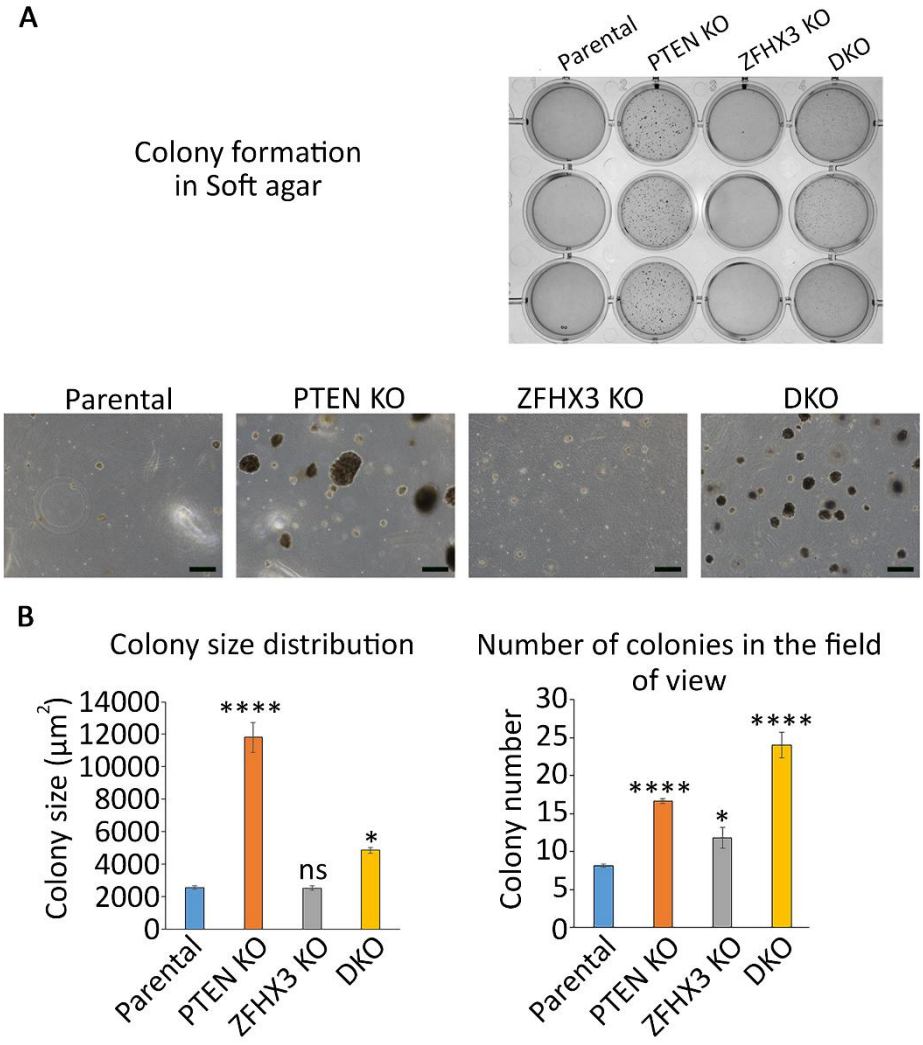

Figure 2. Anchorage independent growth of the genome-edited MCF10A cell lines in soft agar. (**A**) Overall view. Scale bars 200 µm. (**B**) Quantification. Apparent area and numbers of colonies. n=3, ANOVA, * P<0.05, **** P<0.0001, ns not significant.

ZFHX3 KO cells formed more colonies than parental cells, but less than *PTEN* KO cells. All colonies of *ZFHX3* KO cells were of small size. When the two KOs were combined, colony size was intermediate, in between the sizes displayed by the two single KOs. However, the number of colonies increased indicating some synergy in between the two TSGs on this parameter.

2.3. Migration of epithelial islets

To study the behavior of epithelial islets, we recorded sparse cell cultures in the depleted medium. Cells within small islets consisting in 5-10 cells were tracked (Movies S1-4). Trajectories were plotted in a chart where the various cells are registered from the same origin at the center of the graph (Figure 3A). Trajectories highlighted that single *PTEN* KO cells in islets migrated much more actively than cells of other genotype. This is illustrated by the Mean Square Displacement (MSD) that corresponds to the area explored per interval of time (Figure 3B). This higher exploration of *PTEN* KO cells was associated with increases in all parameters that contributed to migration efficiency, namely persistence, directionality and speed (Figure 3C-E). Even though *ZFHX3* KO cells were forming lamellipodia and were actively migrating, they were not coordinated and islets did not move as a whole, unlike *PTEN* KO islets. In DKO cells, *ZFHX3* inactivation suppressed to a large extent, but not completely, the increase in persistence, directionality and cell speed provided by *PTEN* inactivation.

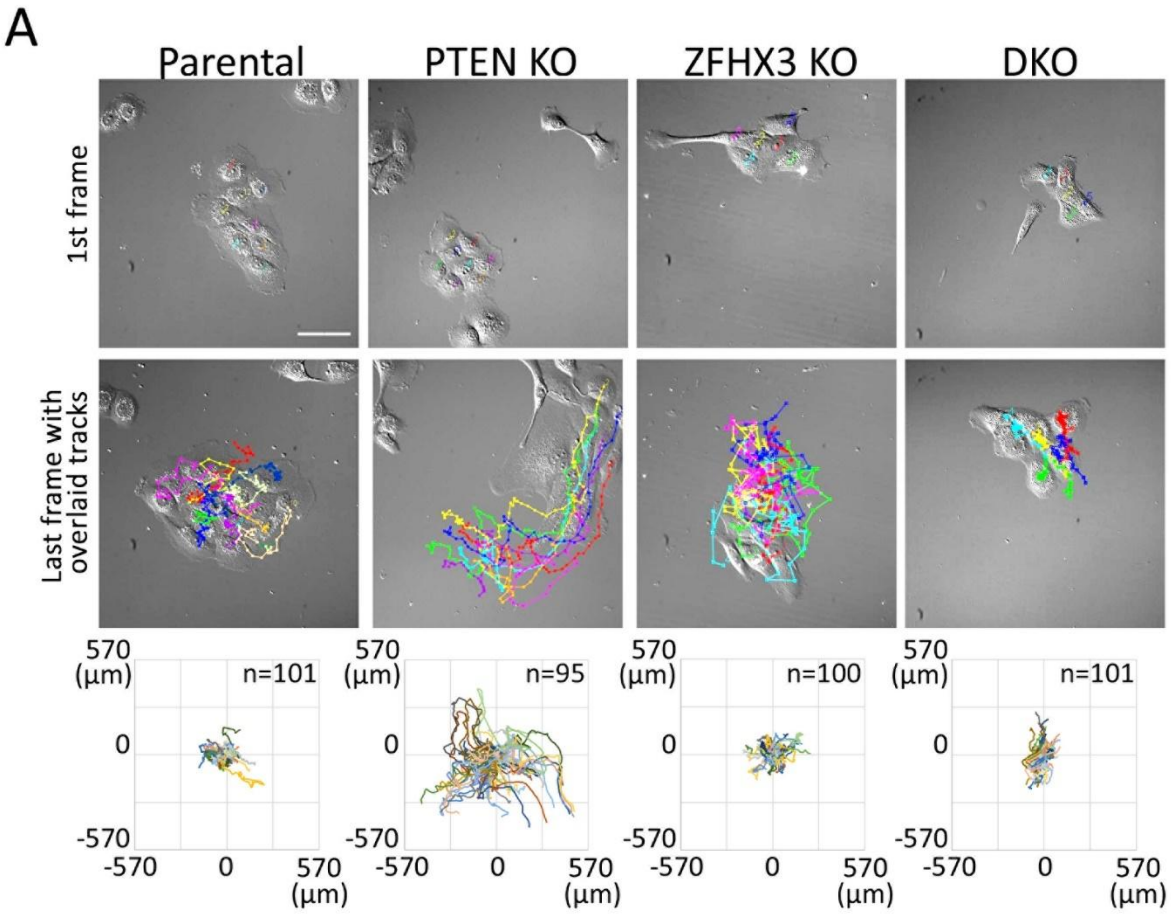

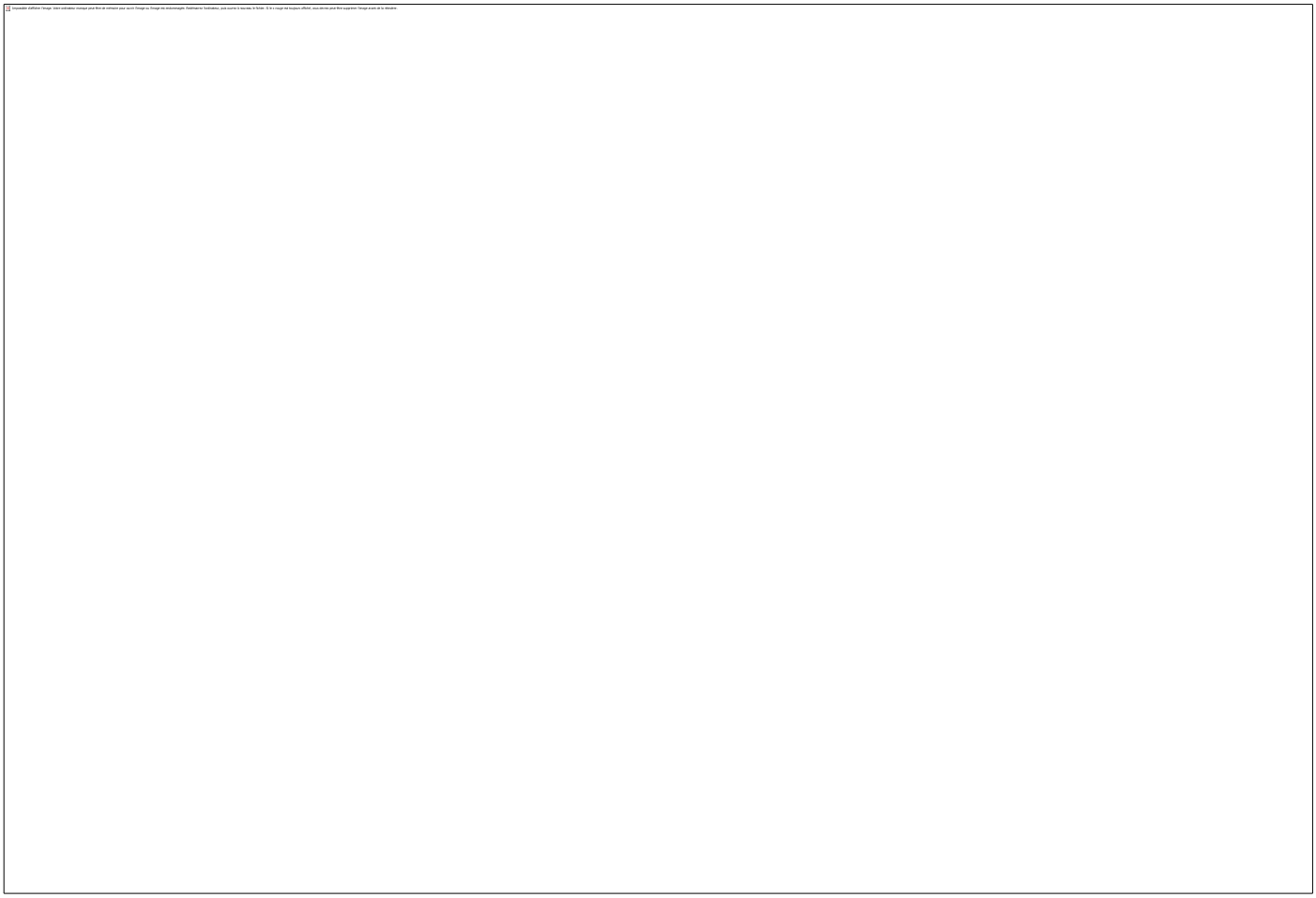

Figure 3. Collective migration of genome-edited MCF10A cell lines within epithelial islets. (**A**) Video frames and cell trajectories. Scale bar: 100 μm. (**B**) a log-log plot of mean square displacements (MSD). (**C**) migration persistence. (**D**) Directionality ratio over elapsed time (16 hours). (**E**) Mean cell speed. 3 independent experiments, more than 100 cells for each line. Mean ± SEM. Kruskal–Wallis test, * $P < 0.05$, ** $P < 0.01$, *** $P < 0.001$, **** $P<0.0001$ and ns: non-significant.

2.4. Influence of PTEN and ZFHX3 KOs on cell motility inside monolayer

As a second approach for migration analysis, we used the experimental wound assay (Figure 4A). *PTEN* KO cells show enhanced healing ability compared to parental cells, while *ZFHX3* KO strongly inhibits the healing process (Figure 4A, B, Movie S5). The DKO displayed a moderately enhanced wound healing compared to parental MCF10A. The velocity-magnitude heat map showed that *PTEN* KO strongly magnifies the speed difference between cells at the wound periphery and cells inside the monolayer, whereas *ZFHX3* KO equalizes front and rear speeds (Figure 4 A, C). DKO cells displayed a front and rear speed difference similar to the parental cells.

To investigate migration coordination, we performed Particle Image Velocimetry (PIV) to display cell flow inside the monolayer and at the wound periphery (Figure 4D). Flow fields for *PTEN* KO showed that cells migrate directionally to close the wound, while *ZFHX3* KO cells flow in multiple directions. However, DKO cells reveal an overall coordinated flow intervened by some uncoordinated areas. To further understand cell coordination, heat maps of the order parameter, i.e. cosine of the angle of displacement vectors with the overall direction of wound closure, were built for each cell line (Figure 4E). In comparison with parental cells, *PTEN* KO enhances the coordination of border cells, making them move more congruently with the overall direction of the wound closure. On the contrary, *ZFHX3* KO cells displayed an uncoordinated pattern of migration of border cells. An intermediate level of coordination was displayed by DKO cells.

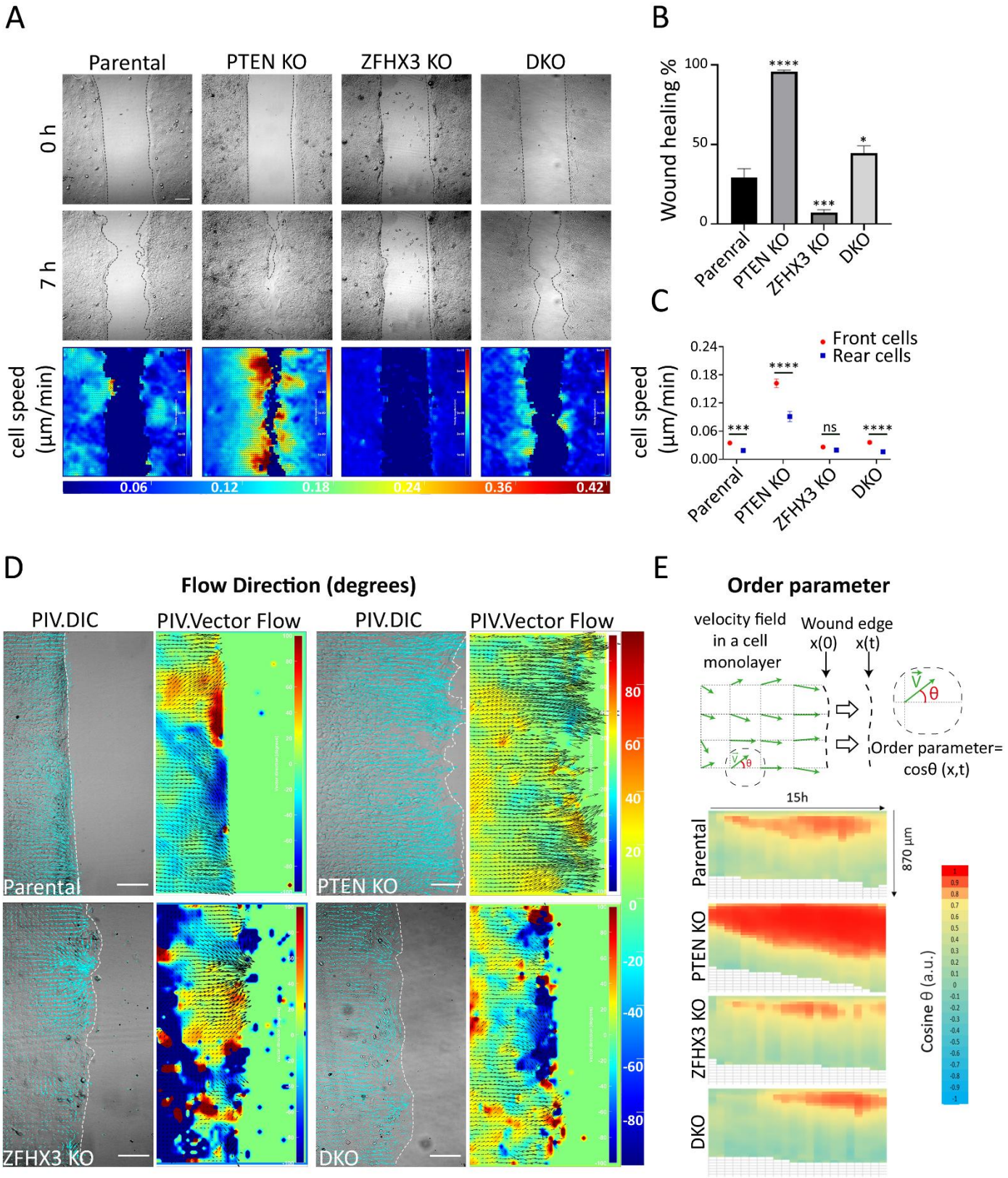

Figure 4. Wound healing of genome-edited MCF10A cell lines. (**A**) Heat map representation of cell speed after 7 h of migration. Scale bars: 100 µm. (**B**) Wound closure percentage after 7 hours. (**C**) Cell speed; for Front and rear cells. (**D**) Heat map representation of cell angles relative to the wound extracted from PIV analysis along the edge at the last hour of migration. Scale bars: 100 µm. (**E**) Local parameter order. Heat map of the average cosine value of the angle of displacement vectors over time. 3 independent experiments. The total sample size more than 15 videos for each cell line. mean ± SEM. Kruskal–Wallis test in Panel B.

Mann-Whitney test for parental and DKO cell lines, unpaired t-test for *PTEN* KO and *ZFHX3* KO cell lines in panel C, * P < 0.05, ** P < 0.01, *** P < 0.001 and **** P<0.0001 and ns non-significant.

Overall, these results show that *ZFHX3* and *PTEN* genes are crucial in controlling collective migration, but their inactivation results in opposite patterns of collective migration regulation. *ZFHX3* KO cells acquire an independent motility pattern with less coordination, whereas *PTEN* KO cells are highly coordinated, thus promoting wound healing.

2.5. Alteration of epithelial characteristics of breast cells upon knockouts of PTEN and ZFHX3

Next, we checked how the alterations of motility behavior caused by KO of *PTEN* and *ZFHX3* are associated with other EMT characteristics. First, we analyzed by Western blot the expression of the EMT markers E-cadherin and vimentin, and as an additional marker, which is more indicative of partial EMT, P-cadherin [35]. The KO of both *PTEN* and *ZFHX3* and their combination did not affect E-cadherin levels (Figure 5 A, B). A small amount of vimentin was expressed by parental MCF10A cells (Figure 5 A). *PTEN* KO decreased vimentin expression, whereas *ZFHX3* KO and DKO cells increased vimentin levels (Figure 5 A, B). P-cadherin levels did not change as a result of *PTEN* and *ZFHX3* KO, but slightly increased in DKO cells, in a non-significant manner (Figure 5 A, B).

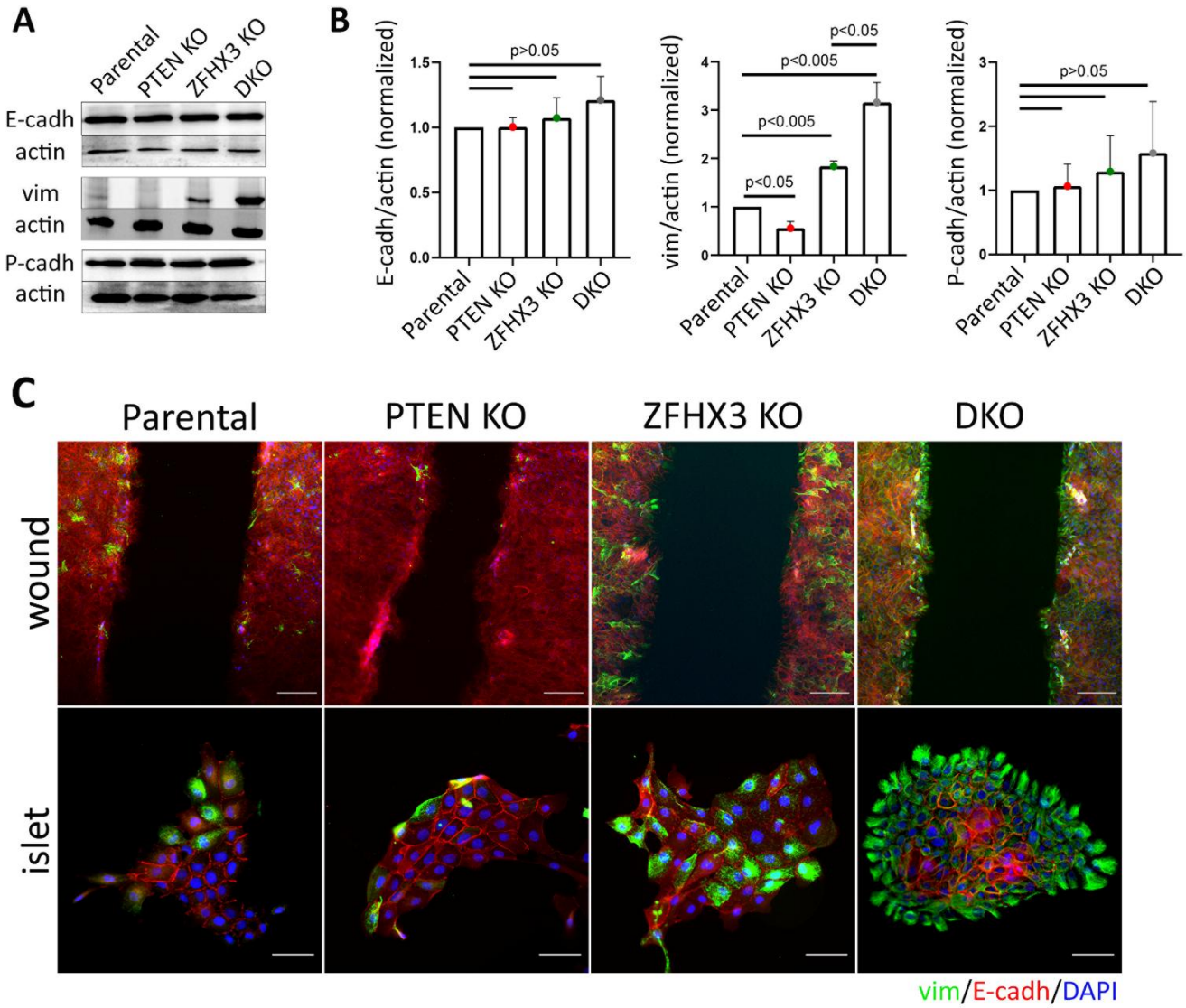

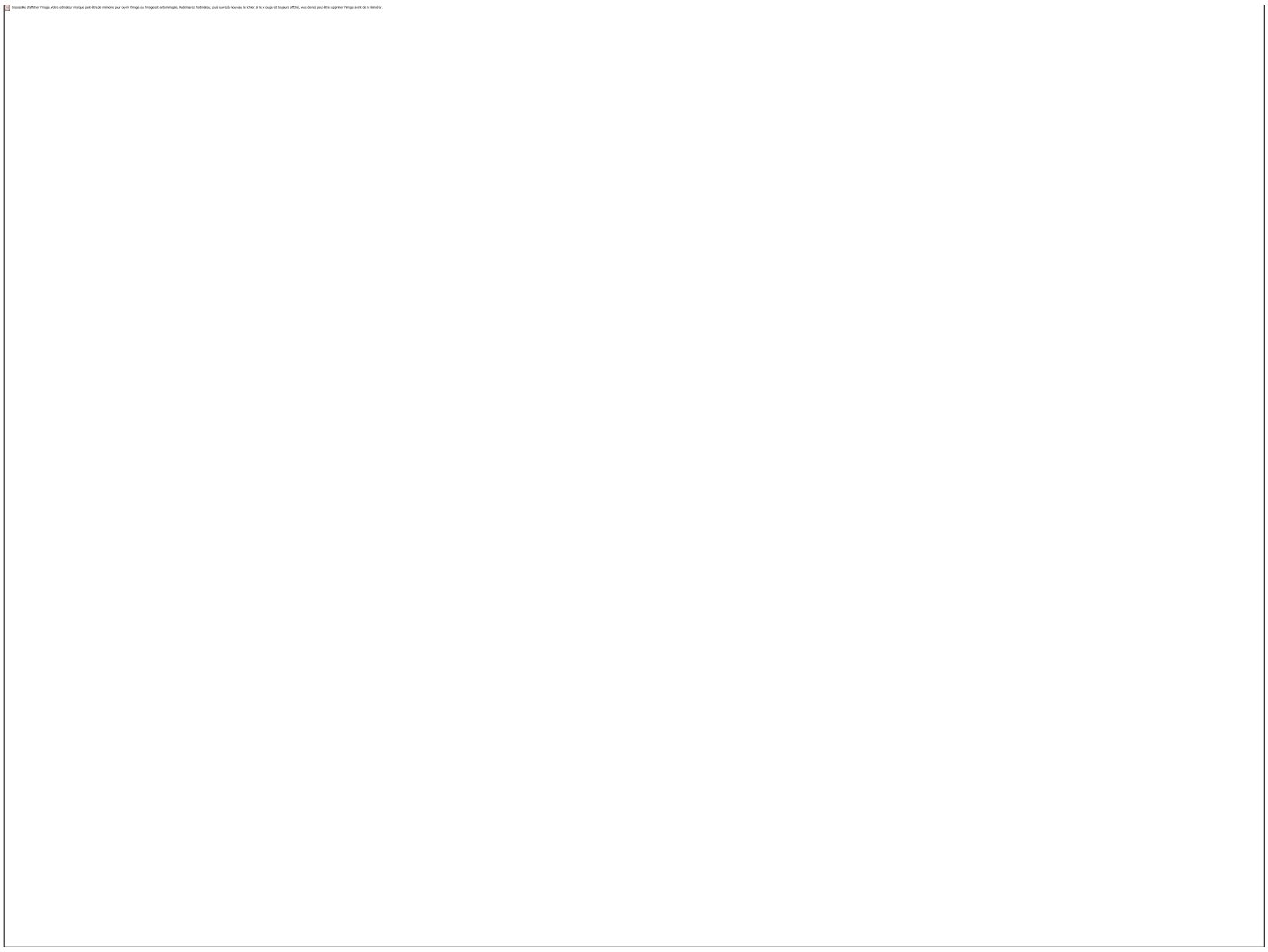

Figure 5. EMT features in genome-edited MCF10A cell lines. (**A**) Western blots of E- and P-cadherins, vimentin and actin. (**B**) Quantification of Western blots by densitometry. Mean ± SEM. 3 independent experiments. (**C**) Immunofluorescence staining of islets and wound edges for vimentin (green), E-cadh (red) and nuclei (blue). Scale bars: 100 μm for wound images and 50 μm for islet images. (**D**) Quantification of vimentin-positive and negative cells within islets or at their periphery. (**E**) Quantification of E-cadherin linear and non-linear junctions within islets of parental and KOs cells. (**F**) Confocal microscopy of E-cadherin immunofluorescence in wound healing experiments. Nuclei are in cyan. Note the radial AJ in *ZFHX3* KO. Arrows indicate the magnified junctions displayed below. Scale bars 18 μm for main immunofluorescence images and 5 μm for magnified junctions. 3 independent experiments. Sample size for each experiment is: parental 193, 236, 438; *PTEN* KO 190, 235, 481; *ZFHX3* KO 150, 264, 424; DKO 250, 289, 356 cells for D. Parental 155, 114, 199; *PTEN* KO 86, 87, 159; *ZFHX3* KO 98, 91, 161; DKO 136, 116, 189 junctions for E. Unpaired t-test in panels B, Contingency Chi square test in D and E. * $P < 0.05$, ** $P < 0.01$, *** $P < 0.001$ and **** $P<0.0001$, ns: non-significant.

We paid special attention to the position of Vimentin positive (Vim+) cells, either inside or at the border of islets. In parental MCF10A, Vim+ cells often localized at the border of islets. The few Vim+ cells in *PTEN* KO cultures also localized at the periphery of islets. In *ZFHX3* KO cultures, the number of Vim+ cells significantly increased both inside and at the periphery of islets. DKO exhibited an additional increase of Vim+ cells, most of which localized at islets periphery (Figure 5 C, D). We also checked the distribution of Vim+ cells in monolayers during wound healing. In parental and *PTEN* KO cultures, most of the few Vim+ cells were localized at the wound edge and only rare Vim+ cells were inside the monolayer (Figure 5 C). *ZFHX3* KO and DKO led to increase in Vim+ cells both inside monolayer and at the wound edge. To address the question of whether the position of Vim+ cells influence wound healing, we analyzed the position of

Vim+ cells in relation with cell motility and wound closure. The presence of Vim+ cells at the wound border was frequently associated with enhanced speed of the Vim- cells surrounding Vim+ cells (Figure S2), raising the possibility that Vim+ cells play a leading role towards Vim- follower cells.

Using confocal microscopy, we checked the morphology of E-cadherin AJs in islets and quantified the different types of junctions. It is sometimes difficult to unambiguously attribute AJ morphology to a category, so we distinguished linear (tangential) AJs, which are typically epithelial, from non-linear AJs, which combine punctuated and radial contacts, and portrays more plastic AJs. The main tendency is that both *PTEN* and *ZFHX3* KO induced rearrangement of AJs, but *PTEN* KO led to the appearance of punctuated E-cadherin adhesions, while *ZFHX3* KO caused the transformation of linear AJs into radial ones. DKO cells exhibited well-pronounced linear AJs (Figure 5E). In cells at the border of monolayers upon wound healing, E-cadherin AJs are not as tight as in between cells further away from the wound, because border cells are actively migrating to close the wound. Nevertheless, at the wound edge, parental MCF10A cells display mostly linear cell-cell AJs, *PTEN* KO cells have condensed dotted lines of E-cadherin (as seen in islets, cf. Figure 1), while *ZFHX3* KO cells exhibit mostly radial AJ (Figure 5F). DKO cells exhibit well pronounced linear AJs with some elements of radial morphology.

Thus, our analysis revealed that *PTEN* and *ZFHX3* knockouts did not induce a complete EMT program, because we did not notice any change in the level of E-cadherin. Also we did not observe altered vimentin levels as a result of *PTEN* KO. At the same time, *PTEN* KO cells display a significantly increased group motility in islets and wound healing. *ZFHX3* KO cells display an increase of vimentin levels, a dramatic change in the morphology of E-cadherin AJs and an increase in the motility of individual cells, yet cells kept E-cadherin AJs. *ZFHX3* KO cells were thus at a more advanced stage of EMT than *PTEN* KO.

3. Discussion

In this work, we have mimicked the inactivation of TSGs that naturally occurs in mammary carcinomas by knocking out these genes in untransformed mammary epithelial cells. *PTEN* inactivation activates the phosphatidylinositol 3-kinase (PI3K) pathway, since *PTEN* encodes the major phosphatase that dephosphorylates the phospholipid PIP3 into PIP2. Activation of the PI3K pathway drives the formation of mammary carcinomas. In fact, activation of the PI3K catalytic subunit by mutations of the *PIK3CA* oncogene is the most frequent alteration of mammary carcinomas [36-38]. *ZFHX3* encodes a transcription factor that controls mammary cell proliferation in response to estrogen signaling [39]. The *ZFHX3* gene is sometimes mutated, more often downregulated in mammary carcinomas [32]. However, we found genetic alterations of *PTEN* and *ZFHX3* in tumors of breast cancer patients. Previously, the same combined inactivation of *ZFHX3* and *PTEN* was found to drive the progression of prostate cancer in a mouse model [40]. The synergy was due to enhanced activation of both PI3K and ERK MAP kinase pathways that promoted proliferation. In our MCF10A cell system, *PTEN* KO was having a more dramatic effect on anchorage-independent growth than *ZFHX3* KO. In these soft agar experiments, we detected a synergy in the number of colonies, but not on their size.

PTEN was previously implicated in the control of cell migration. Its inactivation increases collective migration of tumor cells from colorectal cancer and of primary glial cells [22,26]. The latter effect was independent from its negative role in PI3K signaling. PTEN is dual phosphatase that does not only dephosphorylate the PIP3 phospholipid, but also the Abi1 protein [41]. Abi1 is a subunit of the WAVE regulatory complex (WRC) that activates polymerization of branched actin at the leading edge of migrating cells [42]. When Abi1 phosphorylation is opposed by PTEN, Abi1 is degraded by the calpain protease and the WRC destabilized, thus providing a possible mechanism by which

PTEN loss can promote cell migration [24,41]. In line with previous reports, we found that MCF10A cells knocked out for *PTEN* migrated more persistently in a collective manner. To our knowledge, *ZFHX3* was not previously reported to control cell migration. Here we report that *ZFHX3* KO profoundly uncoordinated collective migration, presumably through its dramatic effect on AJs. The combination of the two KOs indicates that each of the driver gene is dominant over the other for some characteristics, but not all of them (Figure 6).

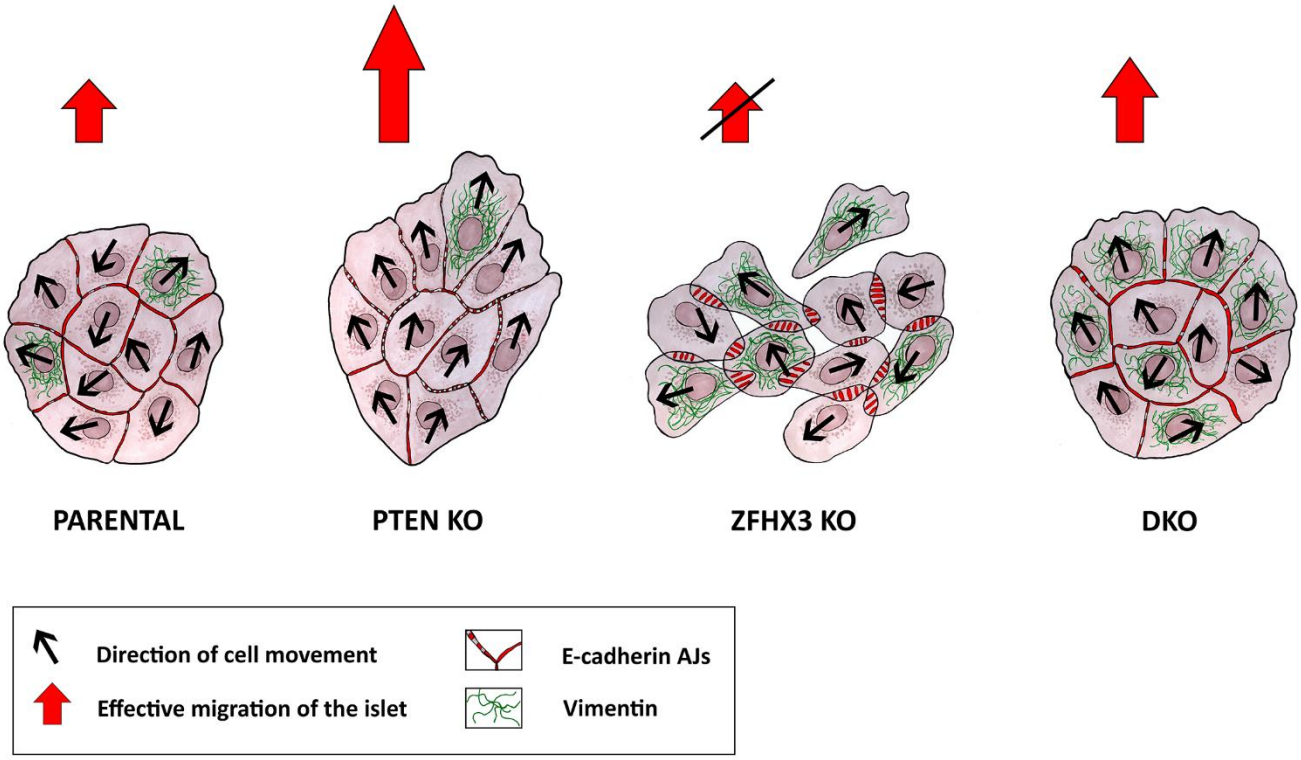

Figure 6. Plasticity of migration modes of genome-edited MCF10A cell lines. KOs of different TSGs induce different stages of partial EMT. *PTEN* KO enhanced collective migration of epithelial islets with linear AJs. *ZFHX3* KO uncoordinated cell motility consistent with their radial AJs and enhanced expression of the mesenchymal marker vimentin. Upon double KO (DKO), cells displayed another motile state, intermediate in terms of collective migration, characterized by linear AJs together with high levels of vimentin.

The migration phenotypes we report for *PTEN* and *ZFHX3* KOs can be interpreted in the framework of partial EMT. We did not observe complete dissociation of MCF10A epithelial cells in association with mesenchymal migration that together would represent a complete EMT. Rather, each KO caused partial EMT at different stages. We found enhanced collective migration of *PTEN* KO epithelial islets and profound rearrangement of AJs in *ZFHX3* KO cells associated with an uncoordinated migration behavior. The other important marker of EMT is altered expression of the mesenchymal marker, vimentin. Vimentin was down-regulated in *PTEN* KO cultures, which behaved overall as a tight but highly motile epithelium, but its expression was retained in fast migrating leader cells of the wound edge in line with enhanced collective migration [43,44]. In *ZFHX3* KO cells, we observed a strong increase in vimentin expression associated with radial E-cadherin positive AJs, two unambiguous signs of EMT [6,45]. It was thus striking to observe linear AJs associated with high vimentin levels in DKO cells, a genuine hybrid phenotype.

Here we have described in detail the complex and subtle modifications in the patterns of migration when two TSGs, *PTEN* and *ZFHX3* were inactivated. *PTEN*

deletion was previously combined with Ras activation, which is frequently observed in tumors [46]. In this work, expression of activated KRAS induced non-directional uncoordinated cell movement that suppressed the enhanced collective migration of PTEN KO cells, as ZFHX3 did in our study. The combination of *PTEN* and *KRAS* genetic alterations led to aggressive tumor cells [47] and the development of lung metastasis [48]. These two examples of *PTEN* inactivation combined with either inactivation of *ZFHX3* or activation of *KRAS* illustrate how migration characteristics are controlled by cancer driver genes that are primarily well established to control cell proliferation and to which extent migration patterns are plastic.

4. Materials and Methods

4.1. Sequencing of invasive mammary carcinomas and putative driver mutations

Ten patients with invasive mammary carcinoma of no special type (luminal subtype, age range 41–67, $T_{1-3}N_{0-2}M_0$ stage) were diagnosed and treated in the Cancer Research Institute of Tomsk NRMC (Tomsk, Russia). DNA was isolated from fresh-frozen tumor (n=10) and peripheral blood samples (n=10) using DNeasy Blood & Tissue kit (Qiagen, USA). DNA and library quality was measured using 2200 TapeStation Instrument (Agilent, USA). Whole exome libraries were prepared using SureSelect XT Human All Exon v7 kit (Agilent, USA) and sequenced on a NextSeq 500 instrument (Illumina, USA). Data were analyzed using the GATK pipeline, and genetic variants were annotated using the ANNOVAR [49,50]. Mutations that were present in peripheral blood were filtered out. Tumor mutations were compared to the oncoKB database of 1020 cancer driver genes downloaded on June 2019.

4.2. Cell culture

PTEN KO (homozygous deletion of exon 2, HD 101-006) and parental MCF10A cells were obtained from Horizon Discovery. Parental MCF10A cells and their derivatives were cultured in DMEM/F12 medium (Gibco) supplemented with 5% horse serum (Hyclone), 100 ng/ml cholera toxin (Sigma), 20 ng/ml epidermal growth factor (Sigma), 0.01 mg/ml insulin (Sigma), 500 ng/ml hydrocortisone (Sigma) and 100 U/ml penicillin/streptomycin (full media).

For Western blot, immunofluorescence and live cell-imaging experiments, cells were seeded into dishes or chambers and cultured in full media overnight, then medium was changed for DMEM/F12 medium (Gibco) supplemented with 1% horse serum (Hyclone), 100 ng/ml cholera toxin (Sigma), 0.01 mg/ml insulin (Sigma), 500 ng/ml hydrocortisone (Sigma) and 100 U/ml penicillin/streptomycin (depleted media without EGF and with 1% horse serum).

After 24 h of incubation in depleted medium, live cell imaging was performed. For live imaging we used depleted DMEM/F12 without phenol red (Sigma, D2906) supplemented with 15 mM HEPES and 1% horse serum. After imaging, cells were fixed and stained for immunofluorescence or lysed for Western blot experiments.

4.3. Generation of KO cell lines

ZFHX3 KO were obtained in parental or *PTEN* KO lines using CRISPR/Cas9 and the following targeting sequence 5′-TCGTCTCGGGGAAGGACAAT-3′ (ThermoFischer CRISPR30279_CR), that covers all known isoforms of ZFHX3. Cells were transfected with crRNA:tracrRNA duplex and the purified Cas9 protein by Lipofectamine CRISPRMAX™ Cas9 transfection reagent (all reagents were from ThermoFisher). Cells were then diluted to 0.8 cells/well into 96 well plates. The presence of mutations was evaluated by direct Sanger sequencing of genomic PCR product. Clones displaying biallelic frameshift mutations were selected for the experiments.

4.4. Anchorage-independent cell growth in soft agar

5000 cells per well of a 12-well plate were embedded in 0.5 ml of 0,35% agar, prepared on full MCF10-A medium. 0.5 ml of 0.8% agar, made on full MCF10A medium, were used as a bottom layer. During 3 weeks of cell growth 0.5 ml of fresh medium were added on the top of soft agar every 4-5 days. Pictures of cell colonies were taken on the Olympus CKX53 microscope supplied with the DP22 camera. Colony size was analysed using the Fiji software.

4.5. Antibodies

For immunofluorescence microscopy mouse monoclonal anti-E-cadherin, clone 36 (BD Transduction Laboratories) and monoclonal anti-vimentin V9 antibodies (Sigma) were used as primary antibodies. Goat polyclonal anti-mouse IgG1 conjugated with AlexaFluor488 and IgG2a conjugated with AlexaFluor 647 (Molecular Probes) were used as secondary antibodies. Nuclei were stained with DAPI (Sigma).

For Western Blot analysis and immunostaining, the following antibodies were used: mouse monoclonal anti-E-cadherin clone 36; mouse monoclonal anti-P-cadherin (BD Transduction Laboratories); monoclonal anti-vimentin V9 antibodies; mouse monoclonal anti-β-actin, clone C4. Horseradish peroxidase-conjugated goat polyclonal anti-mouse IgG antibodies (Jackson ImmunoResearch) were used as secondary antibodies. Other reagents were obtained from Sigma.

4.6. Immunofluorescence

For triple staining for E-cadherin, vimentin and DNA, cells were fixed with 1% paraformaldehyde prepared on DMEM/F12 with 20 mM HEPES at room temperature for 15 min and permeabilized with ice-cold methanol for 3 min at -20°C. The mounted samples were examined with a Leica TCS SP5 confocal laser scanning microscope using the HDX PL APO 100× objective or with a Nikon Eclipse Ti-E microscope using the Plan Fluor 20× objective and ORCA-ER camera (Hamamatsu Photonics) controlled via NIS-Elements AR 3.22 software (Nikon) or with an Axioplan Zeiss epifluorescence microscope using a Plan-Neofluar 100×/1.3 lens (Carl Zeiss, Germany). Vim+ cells and E-cadherin AJs were counted in ImageJ software using the 'cell counter' plugin, and Statistical analysis was performed using GraphPad software with Contingency Chi square test.

4.7. Western Blot

Cells were washed twice with Wash Buffer (10 mM Tris-HCl pH7.5, 0.5 mM EDTA, 150 mM NaCl) and lysed with Lysis Buffer (Wash Buffer supplemented with 0.5% Na deoxycholate, 1% NP-40, protease inhibitor cocktail (Roche), and phosphatase inhibitor cocktail (Sigma)). Samples were mixed with 5x Sample Buffer (250 mM Tris-HCl pH 6.8, 10% SDS, 30% Glycerol, 5% β-mercaptoethanol, 0.02% bromophenol blue), heated for 10 min at 95°C, and loaded onto SDS-polyacrylamide gel in equal protein concentrations according to the SDS-PAGE Bio-Rad protocol. Resolved proteins were transferred to Amersham Hybond-Cnitrocellulose hybridization membranes, 0.45 micron (GE Healthcare, Chicago, IL, USA). Membranes were blocked with 5% m/v bovine serum albumin solution (PanEco, Russia) for further staining of vimentin, or with 5% nonfat milk (AppliChem, Darmstadt, Germany) for further staining of other proteins, in Tris-buffered saline with 0.1% v/v of Tween 20 (AppliChem) for 1 h followed by incubation with the primary antibodies at 4°C overnight. After washing, peroxidase-conjugated secondary antibodies were applied for 1 h at room temperature. Blotted protein bands were detected using Pierce ECL Western Blotting Substrate (ThermoFisher Scientific, Waltham, MA, USA), and chemiluminescence images were captured by Image Quant LAS4000 (GE Healthcare). The densitometry of results was performed in Image J. Statistical analysis was performed in the GraphPad software using unpaired t-test.

4.8. Cell Migration

All live imaging experiments were performed using Nikon Eclipse Ti-E microscope equipped with the Nikon Plan 10× and Plan Apo 20× objectives and ORCA-ER camera (Hamamatsu Photonics) controlled via NIS-Elements AR 3.22 software (Nikon).

Migration of islets

For the analysis of islets migration in sparse culture cells were seeded in 4-well cultivation chambers with glass bottom 155383 (Lab-Tek Thermo Fisher scientific, NY, USA). The time-lapse imaging of cells was performed 24 hours after incubation with the depleted medium. Images were acquired every 10 min for ~16 h. Cell trajectories were obtained by tracking cells with ImageJ and analyzed using the DiPer software [51] to obtain the migration parameters: directional autocorrelation, mean square displacement, average cell speed and single-cell trajectories plotted at the origin. Data from three independent experiments were pooled for the analysis and plotted. The results are expressed as the means and standard errors of the mean (SEM). For migration persistence, a statistical analysis was performed using R. Persistence, measured as movement autocorrelation over time is fit for each cell by an exponential decay with plateau, as described in [52].

$$A = (1 - A_{min}) * e^{-\frac{t}{\tau}} + A_{min}$$

where A is the autocorrelation, t the time interval, A_{min} the plateau and τ the time constant of decay. The plateau value A_{min} is set to zero for cell lines in vitro as they do not display overall directional movement. The time constant τ of exponential fits were then compared using the Kruskal–Wallis test. The average cell speed and directionality were statistically analyzed using GraphPad software with the Kruskal–Wallis test.

Wound healing

To analyze collective cell migration, the wound healing assay was performed using the 2-well silicon inserts (80209, Ibidi) into glass-bottomed dishes. Cells with concentration approximately 3×10^5 cells/ml were seeded inside each well of the insert with the full medium and cultivated overnight. Then, medium was changed to the depleted one (-EGF, 1% horse serum). After 24 hours of incubation in the depleted medium inserts were excluded and the alive-cell-imaging was performed. Images were acquired every 10 min for ~10 h until full wound closing. Using GraphPad software, Means and SEM of wound closure percentages in parental and KOs cells were calculated and statistically analyzed with the Kruskal–Wallis test.

4.9. Analysis of collective cell migration using PIV

Monolayer Heat maps of velocity magnitudes and flow direction inside monolayer were built after performing PIV analysis using the open-source code PIVLab software on MatLab[53,54]. In brief, live cell imaging movies of wound edge (with time lapse 10 minutes) were processed on the PIVLab software using FFT window deformation algorithm with interrogation window of 128 x 128 px (108.8 micron x 108.8 micron) followed by two interrogation passes of 64 x 64 px and 32 x 32 px in second pass and third pass, respectively, with an overlap 50%. Erroneous vectors (shadows) were then filtered using image-based validation filters with a threshold (0.005). Average velocity values of posterior and frontal cells were extracted over 7 hours of migration, results were statistically analyzed in GraphPad software with Mann-Whitney test between front and rear cells in parental and DKO conditions, unpaired t-test between front and rear cells in PTEN KO and ZFHX KO conditions.

Following PIV analysis, an order parameter local mapping was performed by the AVeMap software [55]. Order parameter was defined as a cosine of the angle between each local velocity vector and a normal drawn to the border of a wound. Cell monolayer was divided into 32μm bars, starting from the edge of a wound. Meaning of all cosine

values were averaged within each bar and were plotted in the form of a color kymograph.

Supplementary Materials: The following supporting information can be downloaded at: www.mdpi.com/xxx/s1, Figure S1: *ZFHX3* gene alterations in the single and double KO cell lines studied here. Figure S2: Fast migrating leader cells in *PTEN* KO monolayer express vimentin. Movie S1: Motility of parental MCF10A cells in depleted medium. Movie S2. Motility of *PTEN* KO cells in depleted medium. Movie S3: Motility of *ZFHX3* KO cells in depleted medium. Movie S4: Motility of DKO cells in depleted medium. Movie S5: Wound closure of genome-edited MCF10A cell lines.

Author Contributions: Conceptualization AMG, AYA, EVD; AD performed bulk of the work, analyzed video materials, wrote a draft manuscript, AD together with MEL performed video recordings; AIF, MP, TJ generated ZFHX3 KO and DKO. PIV analysis was done by AD, AIF and JJ; NMN and RSV sequenced tumors and performed bioinformatic analysis of WES data; EVD and AAS analyzed WES data. MEL draw the scheme in Figure 6. AMG and AYA co supervised the project and wrote the paper.

Funding: Work was supported by a grant from Russian Science Foundation # 22-25-00571 to AYA; whole-exome sequencing of breast cancers was supported by RFBR project #18-515-16002 to EVD; work in the AMG lab was supported by a grant from Agence Nationale de la Recherche (ANR-20-CE13-0016-01). The training of MP and TJ in AMG lab benefited from the support of a teaching grant entitled "Personnalized reconstitution of the tumoral process" led by l'X – Ecole polytechnique and Fondation de l'Ecole polytechnique, and sponsored by Servier.

Institutional Review Board Statement: The procedures followed in this study were in accordance with the Helsinki Declaration (1964, amended in 1975 and 1983). This study was approved by the institutional review board, all patients signed an informed consent for voluntary participation, and the number of ethical approval was 10 (29 September 2011).

Informed Consent Statement: Not applicable.

Data Availability Statement: Not applicable.

Acknowledgments: Not applicable.

Conflicts of Interest: The authors declare no conflict of interest.

Abbreviations

AJ: Adherens Junction

EMT: Epithelial-to-Mesenchymal Transition

KO: Knock-Out

LOH: Loss Of Heterozygosity

MSD: Mean Square Displacement

NGS: Next Generation Sequencing

PI3K: PhosphatidylInositol 3-Kinase

PIV: Particle Image Velocimetry

SEM: Standard Error of Mean

TSG: Tumor Suppressor Gene

WES: Whole Exome Sequencing

WRC: WAVE regulatory complex

References

1. Vogelstein, B.; Papadopoulos, N.; Velculescu, V.E.; Zhou, S.; Diaz, L.A., Jr.; Kinzler, K.W. Cancer genome landscapes. *Science* **2013**, *339*, 1546-1558, doi:10.1126/science.1235122.
2. Molinie, N.; Rubtsova, S.N.; Fokin, A.; Visweshwaran, S.P.; Rocques, N.; Polesskaya, A.; Schnitzler, A.; Vacher, S.; Denisov, E.V.; Tashireva, L.A.; et al. Cortical branched actin determines cell cycle progression. *Cell Res* **2019**, *29*, 432-445, doi:10.1038/s41422-019-0160-9.
3. Thiery, J.P. Epithelial-mesenchymal transitions in development and pathologies. *Curr Opin Cell Biol* **2003**, *15*, 740-746, doi:10.1016/j.ceb.2003.10.006.
4. Rubtsova, S.N.; Zhitnyak, I.Y.; Gloushankova, N.A. A Novel Role of E-Cadherin-Based Adherens Junctions in Neoplastic Cell Dissemination. *PLoS One* **2015**, *10*, e0133578, doi:10.1371/journal.pone.0133578.
5. Rubtsova, S.N.; Zhitnyak, I.Y.; Gloushankova, N.A. Phenotypic Plasticity of Cancer Cells Based on Remodeling of the Actin Cytoskeleton and Adhesive Structures. *Int J Mol Sci* **2021**, *22*, doi:10.3390/ijms22041821.
6. Zhitnyak, I.Y.; Rubtsova, S.N.; Litovka, N.I.; Gloushankova, N.A. Early Events in Actin Cytoskeleton Dynamics and E-Cadherin-Mediated Cell-Cell Adhesion during Epithelial-Mesenchymal Transition. *Cells* **2020**, *9*, doi:10.3390/cells9030578.
7. Zhitniak, I.; Glushankova, N.A. [Morphology, cell-cell interactions, and migratory activity of IAR-2 epithelial cells transformed with the RAS oncogene: contribution of cell adhesion protein E-cadherin]. *Ontogenez* **2011**, *42*, 453-464.
8. Pastushenko, I.; Brisebarre, A.; Sifrim, A.; Fioramonti, M.; Revenco, T.; Boumahdi, S.; Van Keymeulen, A.; Brown, D.; Moers, V.; Lemaire, S.; et al. Identification of the tumour transition states occurring during EMT. *Nature* **2018**, *556*, 463-468, doi:10.1038/s41586-018-0040-3.
9. Bornes, L.; Belthier, G.; van Rheenen, J. Epithelial-to-Mesenchymal Transition in the Light of Plasticity and Hybrid E/M States. *J Clin Med* **2021**, *10*, doi:10.3390/jcm10112403.
10. Friedl, P.; Gilmour, D. Collective cell migration in morphogenesis, regeneration and cancer. *Nat Rev Mol Cell Biol* **2009**, *10*, 445-457, doi:10.1038/nrm2720.
11. Lee, J.M.; Dedhar, S.; Kalluri, R.; Thompson, E.W. The epithelial-mesenchymal transition: new insights in signaling, development, and disease. *J Cell Biol* **2006**, *172*, 973-981, doi:10.1083/jcb.200601018.
12. di Bari, M.G.; Ginsburg, E.; Plant, J.; Strizzi, L.; Salomon, D.S.; Vonderhaar, B.K. Msx2 induces epithelial-mesenchymal transition in mouse mammary epithelial cells through upregulation of Cripto-1. *J Cell Physiol* **2009**, *219*, 659-666, doi:10.1002/jcp.21712.
13. Kroger, C.; Afeyan, A.; Mraz, J.; Eaton, E.N.; Reinhardt, F.; Khodor, Y.L.; Thiru, P.; Bierie, B.; Ye, X.; Burge, C.B.; et al. Acquisition of a hybrid E/M state is essential for tumorigenicity of basal breast cancer cells. *Proc Natl Acad Sci U S A* **2019**, *116*, 7353-7362, doi:10.1073/pnas.1812876116.
14. Jolly, M.K.; Somarelli, J.A.; Sheth, M.; Biddle, A.; Tripathi, S.C.; Armstrong, A.J.; Hanash, S.M.; Bapat, S.A.; Rangarajan, A.; Levine, H. Hybrid epithelial/mesenchymal phenotypes promote metastasis and therapy resistance across carcinomas. *Pharmacol Ther* **2019**, *194*, 161-184, doi:10.1016/j.pharmthera.2018.09.007.
15. Novikov, N.M.; Zolotaryova, S.Y.; Gautreau, A.M.; Denisov, E.V. Mutational drivers of cancer cell migration and invasion. *Br J Cancer* **2021**, *124*, 102-114, doi:10.1038/s41416-020-01149-0.
16. Alvarez-Garcia, V.; Tawil, Y.; Wise, H.M.; Leslie, N.R. Mechanisms of PTEN loss in cancer: It's all about diversity. *Semin Cancer Biol* **2019**, *59*, 66-79, doi:10.1016/j.semcancer.2019.02.001.
17. Bonneau, D.; Longy, M. Mutations of the human PTEN gene. *Hum Mutat* **2000**, *16*, 109-122, doi:10.1002/1098-1004(200008)16:2<109::AID-HUMU3>3.0.CO;2-0.

18. Leslie, N.R.; Downes, C.P. PTEN function: how normal cells control it and tumour cells lose it. *Biochem J* **2004**, *382*, 1-11, doi:10.1042/BJ20040825.
19. Garcia, J.M.; Silva, J.; Pena, C.; Garcia, V.; Rodriguez, R.; Cruz, M.A.; Cantos, B.; Provencio, M.; Espana, P.; Bonilla, F. Promoter methylation of the PTEN gene is a common molecular change in breast cancer. *Genes Chromosomes Cancer* **2004**, *41*, 117-124, doi:10.1002/gcc.20062.
20. Lu, Y.M.; Cheng, F.; Teng, L.S. The association between phosphatase and tensin homolog hypermethylation and patients with breast cancer, a meta-analysis and literature review. *Sci Rep* **2016**, *6*, 32723, doi:10.1038/srep32723.
21. Zhang, H.Y.; Liang, F.; Jia, Z.L.; Song, S.T.; Jiang, Z.F. PTEN mutation, methylation and expression in breast cancer patients. *Oncol Lett* **2013**, *6*, 161-168, doi:10.3892/ol.2013.1331.
22. Bowen, K.A.; Doan, H.Q.; Zhou, B.P.; Wang, Q.; Zhou, Y.; Rychahou, P.G.; Evers, B.M. PTEN loss induces epithelial--mesenchymal transition in human colon cancer cells. *Anticancer Res* **2009**, *29*, 4439-4449.
23. Mulholland, D.J.; Kobayashi, N.; Ruscetti, M.; Zhi, A.; Tran, L.M.; Huang, J.; Gleave, M.; Wu, H. Pten loss and RAS/MAPK activation cooperate to promote EMT and metastasis initiated from prostate cancer stem/progenitor cells. *Cancer Res* **2012**, *72*, 1878-1889, doi:10.1158/0008-5472.CAN-11-3132.
24. Qi, Y.; Liu, J.; Chao, J.; Scheuerman, M.P.; Rahimi, S.A.; Lee, L.Y.; Li, S. PTEN suppresses epithelial-mesenchymal transition and cancer stem cell activity by downregulating Abi1. *Sci Rep* **2020**, *10*, 12685, doi:10.1038/s41598-020-69698-1.
25. Chiang, K.C.; Hsu, S.Y.; Lin, S.J.; Yeh, C.N.; Pang, J.H.; Wang, S.Y.; Hsu, J.T.; Yeh, T.S.; Chen, L.W.; Kuo, S.F.; et al. PTEN Insufficiency Increases Breast Cancer Cell Metastasis In Vitro and In Vivo in a Xenograft Zebrafish Model. *Anticancer Res* **2016**, *36*, 3997-4005.
26. Peglion, F.; Capuana, L.; Perfettini, I.; Boucontet, L.; Braithwaite, B.; Colucci-Guyon, E.; Quissac, E.; Forsberg-Nilsson, K.; Llense, F.; Etienne-Manneville, S. PTEN inhibits AMPK to control collective migration. *Nat Commun* **2022**, *13*, 4528, doi:10.1038/s41467-022-31842-y.
27. Cao, L.; Graue-Hernandez, E.O.; Tran, V.; Reid, B.; Pu, J.; Mannis, M.J.; Zhao, M. Downregulation of PTEN at corneal wound sites accelerates wound healing through increased cell migration. *Invest Ophthalmol Vis Sci* **2011**, *52*, 2272-2278, doi:10.1167/iovs.10-5972.
28. Jung, C.G.; Kim, H.J.; Kawaguchi, M.; Khanna, K.K.; Hida, H.; Asai, K.; Nishino, H.; Miura, Y. Homeotic factor ATBF1 induces the cell cycle arrest associated with neuronal differentiation. *Development* **2005**, *132*, 5137-5145, doi:10.1242/dev.02098.
29. Sun, X.; Fu, X.; Li, J.; Xing, C.; Martin, D.W.; Zhang, H.H.; Chen, Z.; Dong, J.T. Heterozygous deletion of Atbf1 by the Cre-loxP system in mice causes preweaning mortality. *Genesis* **2012**, *50*, 819-827, doi:10.1002/dvg.22041.
30. Zhao, D.; Han, X.; Huang, L.; Wang, J.; Zhang, X.; Jeon, J.H.; Zhao, Q.; Dong, J.T. Transcription factor ZFHX3 regulates calcium influx in mammary epithelial cells in part via the TRPV6 calcium channel. *Biochem Biophys Res Commun* **2019**, *519*, 366-371, doi:10.1016/j.bbrc.2019.08.148.
31. Li, M.; Zhang, A.; Zheng, Y.; Li, J.; Zhao, J. ATBF1 Participates in Dual Functions of TGF-beta via Regulation of Gene Expression and Protein Translocalization. *Biomolecules* **2020**, *10*, doi:10.3390/biom10050807.
32. Sun, X.; Zhou, Y.; Otto, K.B.; Wang, M.; Chen, C.; Zhou, W.; Subramanian, K.; Vertino, P.M.; Dong, J.T. Infrequent mutation of ATBF1 in human breast cancer. *J Cancer Res Clin Oncol* **2007**, *133*, 103-105, doi:10.1007/s00432-006-0148-y.
33. Zhang, Z.; Yamashita, H.; Toyama, T.; Sugiura, H.; Ando, Y.; Mita, K.; Hamaguchi, M.; Kawaguchi, M.; Miura, Y.; Iwase, H. ATBF1-a messenger RNA expression is correlated with better prognosis in breast cancer. *Clin Cancer Res* **2005**, *11*, 193-198.

34. Dawson, P.J.; Wolman, S.R.; Tait, L.; Heppner, G.H.; Miller, F.R. MCF10AT: a model for the evolution of cancer from proliferative breast disease. *Am J Pathol* **1996**, *148*, 313-319.
35. Ribeiro, A.S.; Paredes, J. P-Cadherin Linking Breast Cancer Stem Cells and Invasion: A Promising Marker to Identify an "Intermediate/Metastable" EMT State. *Front Oncol* **2014**, *4*, 371, doi:10.3389/fonc.2014.00371.
36. Bachman, K.E.; Argani, P.; Samuels, Y.; Silliman, N.; Ptak, J.; Szabo, S.; Konishi, H.; Karakas, B.; Blair, B.G.; Lin, C.; et al. The PIK3CA gene is mutated with high frequency in human breast cancers. *Cancer Biol Ther* **2004**, *3*, 772-775, doi:10.4161/cbt.3.8.994.
37. Samuels, Y.; Wang, Z.; Bardelli, A.; Silliman, N.; Ptak, J.; Szabo, S.; Yan, H.; Gazdar, A.; Powell, S.M.; Riggins, G.J.; et al. High frequency of mutations of the PIK3CA gene in human cancers. *Science* **2004**, *304*, 554, doi:10.1126/science.1096502.
38. Stemke-Hale, K.; Gonzalez-Angulo, A.M.; Lluch, A.; Neve, R.M.; Kuo, W.L.; Davies, M.; Carey, M.; Hu, Z.; Guan, Y.; Sahin, A.; et al. An integrative genomic and proteomic analysis of PIK3CA, PTEN, and AKT mutations in breast cancer. *Cancer Res* **2008**, *68*, 6084-6091, doi:10.1158/0008-5472.CAN-07-6854.
39. Li, M.; Fu, X.; Ma, G.; Sun, X.; Dong, X.; Nagy, T.; Xing, C.; Li, J.; Dong, J.T. Atbf1 regulates pubertal mammary gland development likely by inhibiting the pro-proliferative function of estrogen-ER signaling. *PLoS One* **2012**, *7*, e51283, doi:10.1371/journal.pone.0051283.
40. Sun, X.; Xing, C.; Fu, X.; Li, J.; Zhang, B.; Frierson, H.F., Jr.; Dong, J.T. Additive Effect of Zfhx3/Atbf1 and Pten Deletion on Mouse Prostatic Tumorigenesis. *J Genet Genomics* **2015**, *42*, 373-382, doi:10.1016/j.jgg.2015.06.004.
41. Qi, Y.; Liu, J.; Chao, J.; Greer, P.A.; Li, S. PTEN dephosphorylates Abi1 to promote epithelial morphogenesis. *J Cell Biol* **2020**, *219*, doi:10.1083/jcb.201910041.
42. Molinie, N.; Gautreau, A. The Arp2/3 Regulatory System and Its Deregulation in Cancer. *Physiol Rev* **2018**, *98*, 215-238, doi:10.1152/physrev.00006.2017.
43. Vilchez Mercedes, S.A.; Bocci, F.; Levine, H.; Onuchic, J.N.; Jolly, M.K.; Wong, P.K. Decoding leader cells in collective cancer invasion. *Nat Rev Cancer* **2021**, *21*, 592-604, doi:10.1038/s41568-021-00376-8.
44. Chen, B.J.; Wu, J.S.; Tang, Y.J.; Tang, Y.L.; Liang, X.H. What makes leader cells arise: Intrinsic properties and support from neighboring cells. *J Cell Physiol* **2020**, *235*, 8983-8995, doi:10.1002/jcp.29828.
45. Usman, S.; Waseem, N.H.; Nguyen, T.K.N.; Mohsin, S.; Jamal, A.; Teh, M.T.; Waseem, A. Vimentin Is at the Heart of Epithelial Mesenchymal Transition (EMT) Mediated Metastasis. *Cancers* **2021**, *13*, doi:10.3390/cancers13194985.
46. Lee, R.M.; Vitolo, M.I.; Losert, W.; Martin, S.S. Distinct roles of tumor associated mutations in collective cell migration. *Sci Rep* **2021**, *11*, 10291, doi:10.1038/s41598-021-89130-6.
47. Thompson, K.N.; Whipple, R.A.; Yoon, J.R.; Lipsky, M.; Charpentier, M.S.; Boggs, A.E.; Chakrabarti, K.R.; Bhandary, L.; Hessler, L.K.; Martin, S.S.; et al. The combinatorial activation of the PI3K and Ras/MAPK pathways is sufficient for aggressive tumor formation, while individual pathway activation supports cell persistence. *Oncotarget* **2015**, *6*, 35231-35246, doi:10.18632/oncotarget.6159.
48. Yankaskas, C.L.; Thompson, K.N.; Paul, C.D.; Vitolo, M.I.; Mistriotis, P.; Mahendra, A.; Bajpai, V.K.; Shea, D.J.; Manto, K.M.; Chai, A.C.; et al. A microfluidic assay for the quantification of the metastatic propensity of breast cancer specimens. *Nat Biomed Eng* **2019**, *3*, 452-465, doi:10.1038/s41551-019-0400-9.
49. Van der Auwera, G.A.; Carneiro, M.O.; Hartl, C.; Poplin, R.; Del Angel, G.; Levy-Moonshine, A.; Jordan, T.; Shakir, K.; Roazen, D.; Thibault, J.; et al. From FastQ data to high confidence variant calls: the Genome Analysis Toolkit best practices pipeline. *Curr Protoc Bioinformatics* **2013**, *43*, 11 10 11-11 10 33, doi:10.1002/0471250953.bi1110s43.

50. Wang, K.; Li, M.; Hakonarson, H. ANNOVAR: functional annotation of genetic variants from high-throughput sequencing data. *Nucleic Acids Res* **2010**, *38*, e164, doi:10.1093/nar/gkq603.
51. Gorelik, R.; Gautreau, A. Quantitative and unbiased analysis of directional persistence in cell migration. *Nat Protoc* **2014**, *9*, 1931-1943, doi:10.1038/nprot.2014.131.
52. Polesskaya, A.; Boutillon, A.; Wang, Y.; Lavielle, M.; Vacher, S.; Schnitzler, A.; Molinie, N.; Rocques, N.; Fokin, A.; Bièche, I. CYFIP2 containing WAVE complexes inhibit cell migration. **2020**.
53. Thielicke, W.; Sonntag, R. Particle Image Velocimetry for MATLAB: Accuracy and Enhanced Algorithms in PIVlab, J. Open Res. Softw., 9. **2021**.
54. Thielicke, W.; Stamhuis, E.J. PIVlab – Towards User-friendly, Affordable and Accurate Digital Particle Image Velocimetry in MATLAB. *Journal of Open Research Software* **2014**, *2*, doi:10.5334/jors.bl.
55. Deforet, M.; Parrini, M.C.; Petitjean, L.; Biondini, M.; Buguin, A.; Camonis, J.; Silberzan, P.J.N.m. Automated velocity mapping of migrating cell populations (AVeMap). **2012**, *9*, 1081-1083.